

# Compton scattering in the Endpoint Model

Sumeet Dagaonkar\*

*Department of Physics, Indian Institute of Technology, Kanpur 208016, India*

## Abstract

We use the Endpoint model for exclusive hadronic processes to study Compton scattering of the proton. The parameters of the Endpoint model are fixed using the data for  $F_1$  and the ratio of Pauli and Dirac form factors ( $F_2/F_1$ ) and then used to get numerical predictions for the differential scattering cross section. We studied the Compton scattering at fixed  $\theta_{CM}$  in the  $s \sim t \gg \Lambda_{QCD}$  limit and at fixed  $s$  much larger than  $t$  limit. We observed that the calculations in the Endpoint Model give a good fit with experimental data in both regions.

Though we have a well understood QCD Lagrangian, predicting processes involving hadrons is a difficult task. The interaction of a high energy probe with quarks or gluons in a hadron requires us to understand physics which is non-perturbative. While in processes like deep inelastic scattering we are able to successfully use factorization - to separate the non-perturbative part into a parton distribution function while the rest could be calculated perturbatively, such simplifications are understood to be much more difficult in the case of exclusive processes [1]. Theoretical models aimed at explaining such processes have been around for four decades now and the ideas can be spilt into two major camps - methods involving hard gluon exchanges within the constituents (short distance model) and methods without hard exchanges (soft or Feynman mechanism). The Endpoint Model (EP) used in this paper combines the idea of soft mechanism with a model of hadron wavefunction which constrains the transverse momenta of confined quarks.

The exclusive process of interest in this paper is the Real Compton scattering ( $p\gamma \rightarrow p\gamma$ ). The first measurements for Compton scattering were made at Cornell [2], where the differential cross section  $d\sigma/dt$  was measured and found to show a scaling of  $1/s^6$ . However more recent measurements at JLab [3] have shown that the scaling goes more like  $1/s^{8.0 \pm 0.2}$ . In recent years the experiments using polarization transfer [4] have also given measurements of transverse polarization transfer  $K_{LS}$  and longitudinal polarization transfer  $K_{LL}$ .

The first theoretical predictions for the scaling behaviour of Compton scattering appeared in [5, 6]. They predicted that  $d\sigma/dt|_{\text{fixed } t} \propto 1/s^6 f(t/s)$  using simple constituent counting ideas. Recent calculations in perturbative QCD (short distance model) [7, 8] using this formalism give predictions a order lower than the experimental data. However, it is understood that the perturbative calculations are only applicable at asymptotically high energies not explored at existing experimental facilities. The soft mechanism was used by Diehl et al.[9] in calculations involving generalized parton distribution functions (GPD), while Miller [10] calculated the handbag diagram in the constituent quark model (CQM). The former work was shown to be equivalent to a sum of overlap of light cone wave functions for all Fock states. For the leading Fock state, the pole structure leads to a similar endpoint dominance as obtained in our model. While the GPD based analysis agrees with some features of the data, the scaling behaviour is not consistent with the

---

\*sumeetkd@iitk.ac.in

latest data. Work by Kivel and Vanderhaeghen [11, 12] on Compton scattering unifies the short distance and the soft mechanism using Soft collinear effective theory.

The latest results on polarization transfer measurements [4] show that, while the  $K_{LS}$  agrees well with the results of pQCD[8], GPD's [13], CQM [10] and SCET [12], the  $K_{LL}$  measurements have been unexpectedly larger and do not agree with any of the theoretical predictions.

The Endpoint Model [14, 15] applies to all exclusive hadronic processes and reproduces the quark counting rules at high energies. In the model, the dominant contributions involve struck quarks carrying a large fraction of the hadron's momenta. The scaling is now completely dependent on the endpoint behaviour of the light cone wavefunctions. It is then possible to obtain the functional form of the wavefunction near the endpoint. After extracting the wavefunction of the proton from the  $F_1$  data, the authors successfully used the wavefunction to understand the scaling behaviour of  $pp$  scattering and the ratio of the Pauli and Dirac form factors ( $F_2(Q^2)/F_1(Q^2)$ ) of the proton. These results motivated the author to attack the Compton scattering problem using the Endpoint Model.

After introducing the Endpoint Model and setting up the frame work, we will show in Section 1 that the EP calculation for  $d\sigma/dt$  obeys scaling laws of [5, 6] at large  $s$  in the  $s \sim t \gg \Lambda_{QCD}$  limit and also a scaling of  $1/t^4$  in the fixed  $s$  much larger than  $t$  region. A detailed numerical calculation in Section 2 will help us determine the range of  $s$  for which we may expect the scaling behaviour to set in and we will also extend the model's prediction into a low  $Q^2$  region to compare with data. At asymptotic energies, we expect that pQCD contributions may dominate. However as seen in the current analysis, a soft mechanism like the Endpoint model can be used to understand data which lies within experimental reach.

## 1 Compton scattering using the Endpoint model

The diagrams allowed for Compton scattering under the Endpoint Model are given in Fig. 1. It can be noticed that the interaction between the struck quark and the photon mirrors the diagrams of the Compton scattering with electrons.

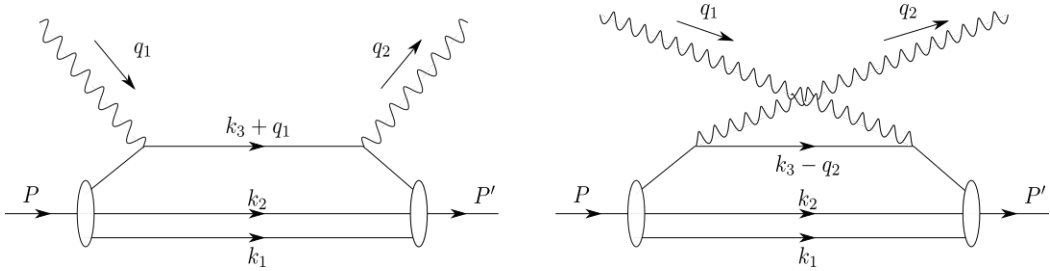


Figure 1: Two diagrams from Compton scattering of proton in the Endpoint Model

### 1.1 Kinematics

In the above diagrams, the incoming proton is understood to be deflected by  $q^\mu = (0, Q, 0, 0)$ , where  $q^\mu = q_1^\mu - q_2^\mu$ . This allows us to use the same frame and kinematics for the proton, as was used for the analysis of Dirac and Pauli form factors [14, 15] with  $q = (0, Q, 0, 0)$ ,  $P = (\sqrt{Q^2/2 + M_P^2}, -Q/2, 0, Q/2)$ ,  $P' = (\sqrt{Q^2/2 + M_P^2}, Q/2, 0, Q/2)$ . We can choose  $q_1, q_2$  appropriately so that  $\theta_{cm} \in [64^\circ, 130^\circ]$ , which is the range of the data obtained at Jlab [3]. For  $\theta_{cm} \approx 90^\circ$ ,  $q_1 = (Q/\sqrt{2}, Q/2, 0, -Q/2)$ ,  $q_2 = (Q/\sqrt{2}, -Q/2, 0, -Q/2)$ .

Let us also define the various quark momenta that will be useful in our calculation, starting with a basis for transverse momenta:  $y^\mu = (0, 0, 1, 0) = y'$  such that  $\hat{P} \cdot y = \hat{P}' \cdot y' = 0$  and  $n^\mu = (1/\sqrt{2})(0, -1, 0, -1)$  such that  $\hat{P} \cdot n = 0$  and  $n'^\mu = (1/\sqrt{2})(0, 1, 0, -1)$  such that  $\hat{P}' \cdot n' = 0$ . Here  $\hat{P} = (0, -1/\sqrt{2}, 0, 1/\sqrt{2})$  and  $\hat{P}' = (0, 1/\sqrt{2}, 0, 1/\sqrt{2})$  are the unit vectors along the direction of propagation of the incoming photon and incoming proton respectively. The four momenta of the quarks are then given by,

$$\begin{aligned} k_i^\mu &= \left( k_i^0, -x_i \frac{Q}{2} - \frac{k_{in}}{\sqrt{2}}, k_{iy}, x_i \frac{Q}{2} - \frac{k_{in}}{\sqrt{2}} \right) \\ k_i'^\mu &= \left( k_i'^0, x_i' \frac{Q}{2} + \frac{k'_{in}}{\sqrt{2}}, k'_{iy}, x_i' \frac{Q}{2} - \frac{k'_{in}}{\sqrt{2}} \right) \end{aligned} \quad (1)$$

## 1.2 Endpoint Model Calculation

The amplitude for the process can be written as

$$\begin{aligned} i\mathcal{M} &= \int \prod_i \frac{d^4 k_i}{(2\pi)^4} \frac{d^4 k_i'}{(2\pi)^4} (2\pi)^4 \delta(k_1 + k_2 + k_3 - P) (2\pi)^4 \delta(k_1' + k_2' + k_3' - P') \\ &\quad \epsilon^{*\mu}(q_2) \epsilon^\nu(q_1) \left[ \overline{\Psi}_{\alpha'\beta'\gamma'}(k_i') \times \mathcal{M}_{\alpha'\beta'\gamma'\alpha\beta\gamma}^{\mu\nu} \times \Psi_{\alpha\beta\gamma}(k_i) \right], \end{aligned} \quad (2)$$

where  $\Psi_{\alpha\beta\gamma}$  refer to 3 quark Bethe-Salpeter wavefunction, the indices  $\alpha, \beta, \gamma$  refer to the  $u, u, d$  carrying momentum  $k_1, k_2, k_3$  respectively. The primed quantities refer to the outgoing proton.

The  $\mathcal{M}^{\mu\nu}$  in the above expression is taken as,

$$\begin{aligned} \mathcal{M}_{\alpha'\beta'\gamma'\alpha\beta\gamma}^{\mu\nu} &= \left[ (-ie_u \gamma^\mu) \frac{i(\not{k}_1 + \not{q}_1 + m_q)}{(k_1 + q_1)^2 - m_q^2} (-ie_u \gamma^\nu) + (-ie_u \gamma^\nu) \frac{i(\not{k}_1 - \not{q}_2 + m_q)}{(k_1 - q_2)^2 - m_q^2} (-ie_u \gamma^\mu) \right]_{\alpha'\alpha} \\ &\quad (2\pi)^{12} \delta^4(k_1 + q - k_1') i(\lambda \not{k}_2 - m_2)_{\beta'\beta} \delta^4(k_2 - k_2') i(\lambda \not{k}_3 - m_3)_{\gamma'\gamma} \delta^4(k_3 - k_3') \\ &+ \left[ (-ie_u \gamma^\mu) \frac{i(\not{k}_2 + \not{q}_1 + m_q)}{(k_2 + q_1)^2 - m_q^2} (-ie_u \gamma^\nu) + (-ie_u \gamma^\nu) \frac{i(\not{k}_2 - \not{q}_2 + m_q)}{(k_2 - q_2)^2 - m_q^2} (-ie_u \gamma^\mu) \right]_{\beta'\beta} \\ &\quad (2\pi)^{12} \delta^4(k_2 + q - k_2') i(\lambda \not{k}_1 - m_1)_{\alpha'\alpha} \delta^4(k_1 - k_1') i(\lambda \not{k}_3 - m_3)_{\gamma'\gamma} \delta^4(k_3 - k_3') \\ &+ \left[ (-ie_d \gamma^\mu) \frac{i(\not{k}_3 + \not{q}_1 + m_q)}{(k_3 + q_1)^2 - m_q^2} (-ie_d \gamma^\nu) + (-ie_d \gamma^\nu) \frac{i(\not{k}_3 - \not{q}_2 + m_q)}{(k_3 - q_2)^2 - m_q^2} (-ie_d \gamma^\mu) \right]_{\gamma'\gamma} \\ &\quad (2\pi)^{12} \delta^4(k_3 + q - k_3') i(\lambda \not{k}_1 - m_1)_{\alpha'\alpha} \delta^4(k_1 - k_1') i(\lambda \not{k}_2 - m_2)_{\beta'\beta} \delta^4(k_2 - k_2'), \end{aligned} \quad (3)$$

where we have taken into account both diagrams in Fig. [1] and the three terms represent the photon's interactions with u,u,d quarks respectively.

We would like to integrate over the  $k_i^-, k_i'^-$  momenta in the Eq. 3 so as to replace the Bethe Salpeter wavefunctions by Light cone wavefunctions using the approximations developed in [16]. The integrand has  $k_i^-, k_i'^-$  dependence due to the propagators associated with the Bethe Salpeter wavefunction and from the spectator quarks. The spectator quarks interact through soft gluons and behave like a effective diquark propagator. Its form will require us to do an detailed analysis of the physics in this non-perturbative system. As a starting point however, we use a simple model consisting of two non-interacting quarks given by  $(\lambda \not{k}_2 - m)(\lambda \not{k}_3 - m)$ , where  $\lambda$  may be a scalar function of the spectator quark momentum  $(k_2, k_3)$ . The complete expression for  $\mathcal{M}^{\mu\nu}$  is assumed to be dominated by a region where the quarks are on-shell which allows us to make the substitution  $\kappa_i^- = (k^0 - x_i Q/\sqrt{2})(P^0 + Q/\sqrt{2}) = (m_i^2 + \vec{k}_\perp^2)/(k^0 + x_i Q/\sqrt{2})$ . In this substitution,

we have taken into account the energy scale dependence of the mass which causes the effective mass to be  $m_i^2 \sim \Lambda^2$  for the spectator quarks and  $m_i^2 \sim \text{few MeV}$  for the struck quark. Momenta for each of the quarks is conserved independently and as per the definition of  $i\mathcal{M}$ , a factor of  $\delta^4(P + q_1 - q_2 - P')$  has to be dropped in the above expression.

Under these approximations, the amplitude 2 becomes

$$i\mathcal{M} = \int \prod_i dx_i d\vec{k}_{\perp i} dx'_i d\vec{k}'_{\perp i} \delta(x_1 + x_2 + x_3 - 1) \delta^2(k_{\perp 1} + k_{\perp 2} + k_{\perp 3}) \delta(x'_1 + x'_2 + x'_3 - 1) \delta^2(k'_{\perp 1} + k'_{\perp 2} + k'_{\perp 3}) \epsilon^{*\mu}(q_2) \epsilon^\nu(q_1) \left[ \bar{Y}'_{\alpha' \beta' \gamma'}(x'_i, \vec{k}'_{\perp i}) \times \mathcal{M}_{\alpha' \beta' \gamma' \alpha \beta \gamma}^{\mu\nu} \times Y_{\alpha \beta \gamma}(x_i, \vec{k}_{\perp i}) \right] \quad (4)$$

The light cone wave function for the proton  $Y(k_i)$  at leading twist and leading power of large  $P$  is [17, 18],

$$Y_{\alpha \beta \gamma}(k_i, P) = \frac{f_N}{16\sqrt{2}N_c} \{ (\not{P}C)_{\alpha \beta} (\gamma_5 N)_\gamma \mathcal{V} + (\not{P}\gamma_5 C)_{\alpha \beta} N_\gamma \mathcal{A} + i(\sigma_{\mu\nu} P^\nu C)_{\alpha \beta} (\gamma^\mu \gamma_5 N)_\gamma \mathcal{T} \}. \quad (5)$$

Here  $\mathcal{V}, \mathcal{A}, \mathcal{T}$  are scalar wavefunctions of the quark momenta,  $N$  is the proton spinor,  $N_c$  the number of colors,  $C$  the charge conjugation operator,  $\sigma_{\mu\nu} = \frac{i}{2}[\gamma_\mu, \gamma_\nu]$ , and  $f_N$  is a normalization. The functional dependence for the scalar functions near the endpoint region of the  $x_i$ , the momentum fraction of the struck quark, was obtained in [14] by matching the EP calculation with the experimental scaling behaviour of  $F_1$  of the proton. We will carry over that form in this paper

$$\mathcal{V} = v(1 - x_i) e^{-k_T^2/\Lambda^2}; \quad \mathcal{A} = a(1 - x_i) e^{-k_T^2/\Lambda^2}; \quad \mathcal{T} = t(1 - x_i) e^{-k_T^2/\Lambda^2}. \quad (6)$$

The  $\vec{k}_T$  represents the transverse momenta of the quark which is suppressed by an exponential function in the above form and is understood to be cut off sharply for  $|k_T| > \Lambda_{QCD}$ .

### 1.3 Scaling in Endpoint Model

Before presenting the endpoint model's prediction for Compton scattering, we explicitly evaluate a part of the entire expression to extract the scaling behaviour to be expected for fixed  $\theta_{CM}$  and fixed  $s$  cases.

Let us concentrate on the diagram shown in Fig. 1, in which  $d$  quark is struck. The delta functions in the last term of Eq. 3 and Eq. 4 imply,  $x_1 = 1 - x_2 - x_3; x'_1 = 1 - x'_2 - x'_3; k_{1n} = -k_{2n} - k_{3n}; k_{1y} = -k_{2y} - k_{3y}; k'_{1n} = -k'_{2n} - k'_{3n}; k'_{1y} = -k'_{2y} - k'_{3y}; k_{2y} = k'_{2y}; k_{3y} = k'_{3y}; x'_2 = x_2; x'_3 = x_3; k_{3n} = Q(1 - x'_3)/\sqrt{2}; k'_{3n} = Q(1 - x_3)/\sqrt{2}; k_{2n} = Q(-x'_2)/\sqrt{2}; k'_{2n} = Q(-x_2)/\sqrt{2}$ .

Integrating over the delta functions leads to a factor of  $1/Q^2$ . Using only the first term of the wavefunction Eq. 5, the amplitude is obtained as,

$$i\mathcal{M} = \int dx_1 dx_2 dk_{1y} dk_{2y} \frac{1}{Q^2} \epsilon^{*\mu}(q_2) \epsilon^\nu(q_1) \left[ [(C^{-1} \not{P}')_{\alpha' \beta'} (\bar{N} \gamma_5)_{\gamma'} \mathcal{V}^*] \left[ (-ie_d \gamma^\mu) \frac{i(\not{k}_3 + \not{q}_1 + m_q)}{(k_3 + q_1)^2 - m_q^2} (-ie_d \gamma^\nu) + (-ie_d \gamma^\nu) \frac{i(\not{k}_3 - \not{q}_2 + m_q)}{(k_3 - q_2)^2 - m_q^2} (-ie_d \gamma^\mu) \right]_{\gamma' \gamma} \right] i(\lambda \not{k}_1 - m_1)_{\alpha' \alpha} i(\lambda \not{k}_2 - m_2)_{\beta' \beta} [(\not{P}C)_{\alpha \beta} (\gamma_5 N)_\gamma \mathcal{V}] + \dots \quad (7)$$

The experimentally measured quantity is the unpolarized differential cross section  $d\sigma/dt = 1/16\pi(s -$

$m_p^2)^{1/4} \sum |M|^2$ , (the integrations in the complex conjugate are over the hatted variables)

$$\begin{aligned}
\frac{d\sigma}{dt} &= \frac{1}{16\pi(s-m_p^2)^2} \frac{1}{4} \int dx_1 dx_2 dk_{1y} dk_{2y} \frac{1}{Q^2} \int d\hat{x}_1 d\hat{x}_2 d\hat{k}_{1y} d\hat{k}_{2y} \frac{1}{Q^2} \\
&\left[ \text{Tr}[(C^{-1}(\not{P}'))(\lambda\hat{k}_2 - m_2)(\not{P}C)^\dagger(\lambda\hat{k}_1 - m_1)^\dagger] \text{Tr}[(C^{-1}(\not{P}'))(\lambda\hat{k}_2 - m_2)(\not{P}C)^\dagger(\lambda\hat{k}_1 - m_1)^\dagger]^* \right. \\
&\text{Tr} \left[ (\not{P}' + m_p)\gamma_5 \left[ \frac{\gamma^\mu(\hat{k}_3 + \hat{q}_1 + m_q)\gamma^\nu}{(k_3 + q_1)^2 - m_q^2} + \frac{\gamma^\nu(\hat{k}_3 - \hat{q}_2 + m_q)\gamma^\mu}{(k_3 - q_2)^2 - m_q^2} \right] \gamma_5 (\not{P} + m_p)\gamma_5 \right. \\
&\left. \left[ \frac{\gamma^{\nu'}(\hat{k}_3 + \hat{q}_1 + m_q)\gamma^{\mu'}}{(\hat{k}_3 + q_1)^2 - m_q^2} + \frac{\gamma^{\mu'}(\hat{k}_3 - \hat{q}_2 + m_q)\gamma^{\nu'}}{(\hat{k}_3 - q_2)^2 - m_q^2} \right] \gamma_5 \right] e_d^4 \mathcal{V}^*(k'_i) \mathcal{V}(k_i) \mathcal{V}^*(\hat{k}'_i) \mathcal{V}(\hat{k}_i) + \dots \left. \right] \\
&\sum_{\text{polarization}} \epsilon_\mu^*(q_2) \epsilon_{\mu'}(q_2) \sum_{\text{polarization}} \epsilon_\nu^*(q_1) \epsilon_{\nu'}(q_1). \tag{8}
\end{aligned}$$

We can integrate over the variables after plugging in the wavefunction from Eq. 6. Our calculation shows scaling behaviour in two limits, for  $s \sim t \gg \Lambda_{QCD}$  and for fixed  $s$  much larger than  $t$ . In the  $s \sim t \gg \Lambda_{QCD}$  limit, the leading order contributions give,

$$\begin{aligned}
\frac{d\sigma}{dt} &\sim \int dx_1 dx_2 dk_{1y} dk_{2y} \int d\hat{x}_1 d\hat{x}_2 d\hat{k}_{1y} d\hat{k}_{2y} \frac{1}{16\pi(s-m_p^2)^2} \left( \frac{1}{Q^2} \right)^2 ((P \cdot P')(k_1 \cdot k_2) + \dots) \times \\
&((P \cdot P')(\hat{k}_1 \cdot \hat{k}_2) + \dots) \frac{((k_3 \cdot P)(\hat{k}_3 \cdot P') + \dots)}{(k_3 \cdot q_1)(\hat{k}_3 \cdot q_2)} (1 - x_3)^2 (1 - \hat{x}_3)^2 + \dots \\
&\sim \frac{1}{s^2} \left( \frac{1}{Q^2} \right)^2 (Q^2)^2 \frac{1}{(Q^2)^2} \frac{1}{Q^4} \frac{1}{Q^4} \sim \frac{1}{s^2} \times \frac{1}{s^2} \times \frac{1}{s^2} \times \frac{1}{s^2} \sim \frac{1}{s^6}. \tag{9}
\end{aligned}$$

Thus in the large  $s$  limit, we can see that we obtain a scaling behavior of  $1/s^6$ , as expected from the quark counting rules.

In order to analyse the differential cross section for fixed  $s$  when  $s > t$ , we have to alter the photon momenta defined specifically for  $\theta_{CM} = 90^\circ$  above and instead use  $q_1 = (Q/\sqrt{2}, Q/2, 0, f(s, Q))$ ,  $q_2 = (Q/\sqrt{2}, -Q/2, 0, f(s, Q))$ . The definition of  $s = (P + q_1)^2$  can be used to find the functional form of  $f(s, t)$ . To the leading order in  $s$ , it can be shown that  $f(s, Q) \sim \pm s/Q$ . In the  $s > t$  limit, the leading order contributions are now,

$$\begin{aligned}
\frac{d\sigma}{dt} &\sim \int dx_1 dx_2 dk_{1y} dk_{2y} \int d\hat{x}_1 d\hat{x}_2 d\hat{k}_{1y} d\hat{k}_{2y} \frac{1}{16\pi(s-m_p^2)^2} \left( \frac{1}{Q^2} \right)^2 ((P \cdot P')(k_1 \cdot k_2) + \dots) \times \\
&((P \cdot P')(\hat{k}_1 \cdot \hat{k}_2) + \dots) \frac{((q_2 \cdot P)(q_1 \cdot P') + \dots)}{(k_3 \cdot q_1)(\hat{k}_3 \cdot q_2)} (1 - x_3)^2 (1 - \hat{x}_3)^2 + \dots \\
&\sim \frac{1}{s^2} \left( \frac{1}{Q^2} \right)^2 (Q^2)^2 \frac{s^2}{s^2} \frac{1}{Q^4} \frac{1}{Q^4} \sim \frac{1}{Q^4} \times \frac{1}{Q^4} \sim \frac{1}{Q^8} \sim \frac{1}{t^4} \tag{10}
\end{aligned}$$

## 2 Comparing Compton scattering in Endpoint Model with experimental data

The full prediction of the Endpoint Model for Compton scattering involves substituting the full expressions Eq. 3, 5 into the expression Eq. 8. The expression involves multiple traces over gamma matrices which were handled by the Mathematica package FEYNALC [19]. The resulting

expression contains thousands of terms for each combination of wavefunction  $\mathcal{V}, \mathcal{A}, \mathcal{T}$ . Due to the large number of terms, analytic evaluation would be cumbersome and it is dealt with using a Monte Carlo routine for integration (VEGAS [20]).

In the previous work on Endpoint Model [14], the authors concentrated on explaining the scaling behaviour of exclusive hadronic processes using a functional form of the wavefunction. In the current paper, we extended the above work by using  $\chi^2$  minimization to extract the free parameters of the model. This would be essential when comparing the magnitude of the prediction of the Compton scattering in EP with data. Using the data for  $F_1$ [21] and  $F_2/F_1$ [22, 23](at  $Q^2 \gtrsim 5.5 \text{ GeV}^2$ ) and the EP prediction in [15], the minimization gives the values for the constants  $v, a, t$  from Eq. 6, mass of the quark  $m$  and the factor  $\lambda$  for the model of spectator quarks. The constants obtained in the above minimization will carry over to all the processes that EP may be applied to.

At fixed  $s$  much larger than  $t$ , we observed that the experimental data showed a scaling behaviour of  $1/t^4$  at lower angles. We carried out EP calculations at  $s = 6.79, 8.90, 10.92 \text{ GeV}^2$  and observed that the scaling can be correctly reproduced by the model as was also seen in the calculation in Sec 1.3. We can see in Fig. 2 that there is a good agreement between the data and our EP prediction at the above energies, which improves as we increase the  $s$  of the data. The rise in the  $d\sigma/dt$  at larger angles is however not captured by the EP calculation. Our choice of  $\theta_{CM} = 90^\circ$  in the fixed  $\theta_{CM}$  analysis above was influenced by this disagreement.

For the fixed  $\theta_{cm}$  analysis in the  $s \sim t$  region, the expected scaling behaviour from the quark counting rules [5, 6] was  $1/s^6$  and is not seen in the experimental data which shows a scaling of  $1/s^8$ [3]. We evaluate the integral in Eq. 8 for a range of  $Q^2$  at  $\theta_{CM} = 90^\circ$  and we observe in the resulting plot (Fig. 3) that EP shows the above scaling behaviour of  $1/s^6$  after we reach  $s \sim 25 \text{ GeV}^2$ . At the experimental energy levels, though a  $1/s^8$  scaling was not observed, there was a remarkable match between the EP predictions and the experimental data.

### 3 Conclusions

The Endpoint model combines the soft mechanism and the nature of the transverse momenta of a quark in a hadron to study scaling behaviour in its exclusive processes. Using the model to calculate exclusive processes leads to expressions dominated by the endpoint region of the wavefunction, this helps us extract the nature of the wavefunction. Specifically for the proton, using one set of data to obtain the wavefunction ( $F_1$  data), the scaling behaviour of  $F_2/F_1$  of proton and  $pp$  scattering was successfully obtained. The successes of the Endpoint model lead us to the problem of real Compton scattering of the proton.

The experimental data for Compton scattering [3] show a scaling behaviour for the differential scattering cross section in two regions of  $s, t$ : a  $1/s^8$  scaling for fixed  $\theta_{CM}$  and  $s \sim t \gg \Lambda_{QCD}$  and a  $1/t^4$  scaling at fixed  $s$  much larger than  $t$ . Fixing the free parameters in the Endpoint Model using the data for  $F_1$  and  $F_2/F_1$ , we carried out numerical calculation for Compton scattering in these limits. For fixed  $s$  larger than  $t$ , the Endpoint calculations show the  $1/t^4$  scaling observed in data and have a good match with the data for lower angles. In the fixed  $\theta_{CM}$  and  $s \sim t \gg \Lambda_{QCD}$  region, the Endpoint Model calculation for the Compton scattering shows the elusive  $1/s^6$  scaling, that is expected from constituent counting rules [5, 6]. Moreover, the Endpoint model also suggests that the  $1/s^6$  scaling can be expected to be dominant after  $s \sim 25 \text{ GeV}^2$ . At the experimental values of  $s$ , though the experimentally observed scaling is absent in the Endpoint Model, an excellent agreement with experimental observations can be seen when extending the calculation to lower  $s$  (lower  $Q^2$ ).

With the current work, we have shown once again that the Endpoint model is capable of explaining a range of scaling laws for hadronic processes. It is capable of generating the quark counting rules [5, 6] and also suggests the energy scales at which one can expect these scaling laws to dominate. Fixing the parameters of the model using existing data, the Endpoint model is also able to give an excellent match with experimental data.

As we go to higher angles in the fixed  $s$  differential cross section measurements, EP does not correctly predict the rise in the  $d\sigma/dt$  which has to be explored in future work. Also, further work will be required for the evaluation of polarization transfer variables ( $K_{LL}$  &  $K_{LS}$ ) under the Endpoint model.

## Acknowledgement

The author would like to thank Prof. Pankaj Jain for useful discussions and comments. For the computational work in this paper, I would like to thank the Physics Department at IIT Kanpur for facilities provided. The author would also like to thank Bogdan Wojtsekhowski for suggesting the Compton scattering problem.

## References

- [1] N. Isgur and C. H. Llewellyn Smith, Phys. Rev. Lett. **52** (1984) 1080. doi:10.1103/PhysRevLett.52.1080
- [2] M. A. Shupe *et al.*, Phys. Rev. D **19** (1979) 1921. doi:10.1103/PhysRevD.19.1921
- [3] A. Danagoulian *et al.* [Hall A Collaboration], Phys. Rev. Lett. **98** (2007) 152001 [nucl-ex/0701068 [NUCL-EX]].
- [4] C. Fanelli *et al.*, Phys. Rev. Lett. **115** (2015) no.15, 152001 doi:10.1103/PhysRevLett.115.152001 [arXiv:1506.04045 [nucl-ex]].
- [5] S. J. Brodsky and G. R. Farrar, Phys. Rev. Lett. **31** (1973) 1153. doi:10.1103/PhysRevLett.31.1153
- [6] V. A. Matveev, R. M. Muradian and A. N. Tavkhelidze, Lett. Nuovo Cim. **7** (1973) 719. doi:10.1007/BF02728133
- [7] T. C. Brooks and L. J. Dixon, Phys. Rev. D **62** (2000) 114021 doi:10.1103/PhysRevD.62.114021 [hep-ph/0004143].
- [8] R. Thomson, A. Pang and C. R. Ji, Phys. Rev. D **73** (2006) 054023 doi:10.1103/PhysRevD.73.054023 [hep-ph/0602164].
- [9] M. Diehl, T. Feldmann, R. Jakob and P. Kroll, Eur. Phys. J. C **8** (1999) 409 doi:10.1007/s100529901100 [hep-ph/9811253].
- [10] G. A. Miller, Phys. Rev. C **69** (2004) 052201 doi:10.1103/PhysRevC.69.052201 [nucl-th/0402092].

- [11] N. Kivel and M. Vanderhaeghen, Nucl. Phys. B **883** (2014) 224 doi:10.1016/j.nuclphysb.2014.03.019 [arXiv:1312.5456 [hep-ph]].
- [12] N. Kivel and M. Vanderhaeghen, Eur. Phys. J. C **75** (2015) no.10, 483 doi:10.1140/epjc/s10052-015-3694-0 [arXiv:1504.00991 [hep-ph]].
- [13] H. W. Huang, P. Kroll and T. Morii, Eur. Phys. J. C **23** (2002) 301 Erratum: [Eur. Phys. J. C **31** (2003) 279] doi:10.1007/s100520100883 [hep-ph/0110208].
- [14] S. K. Dagaonkar, P. Jain and J. P. Ralston, Eur. Phys. J. C **74**, no. 8, 3000 (2014) doi:10.1140/epjc/s10052-014-3000-6 [arXiv:1404.5798 [hep-ph]].
- [15] S. Dagaonkar, P. Jain and J. P. Ralston, Eur. Phys. J. C **76** (2016) no.7, 368 doi:10.1140/epjc/s10052-016-4224-4 [arXiv:1503.06938 [hep-ph]].
- [16] S. J. Brodsky, C. R. Ji and M. Sawicki, Phys. Rev. D **32** (1985) 1530.
- [17] V. M. Belyaev and B. L. Ioffe, Zh. Eksp. Teor. Phys. **83**, 876 (1982) [Sov. Phys. JETP 56, 493 (1982)].
- [18] V.A. Avdeenko, V.L. Chernyak and S.A. Korenblit, Yad. Fiz. **33** (1981) 481.
- [19] R. Mertig, M. Bohm and A. Denner, Comput. Phys. Commun. **64** (1991) 345.
- [20] G. P. Lepage, J. Comput. Phys. **27** (1978) 192. doi:10.1016/0021-9991(78)90004-9
- [21] A. F. Sill *et al.*, Phys. Rev. D **48** (1993) 29. doi:10.1103/PhysRevD.48.29
- [22] A. J. R. Puckett, E. J. Brash, M. K. Jones, W. Luo, M. Meziane, L. Pentchev, C. F. Perdrisat and V. Punjabi *et al.*, Phys. Rev. Lett. **104** (2010) 242301 [arXiv:1005.3419 [nucl-ex]].
- [23] A. J. R. Puckett, E. J. Brash, O. Gayou, M. K. Jones, L. Pentchev, C. F. Perdrisat, V. Punjabi and K. A. Aniol *et al.*, Phys. Rev. C **85** (2012) 045203 [arXiv:1102.5737 [nucl-ex]].



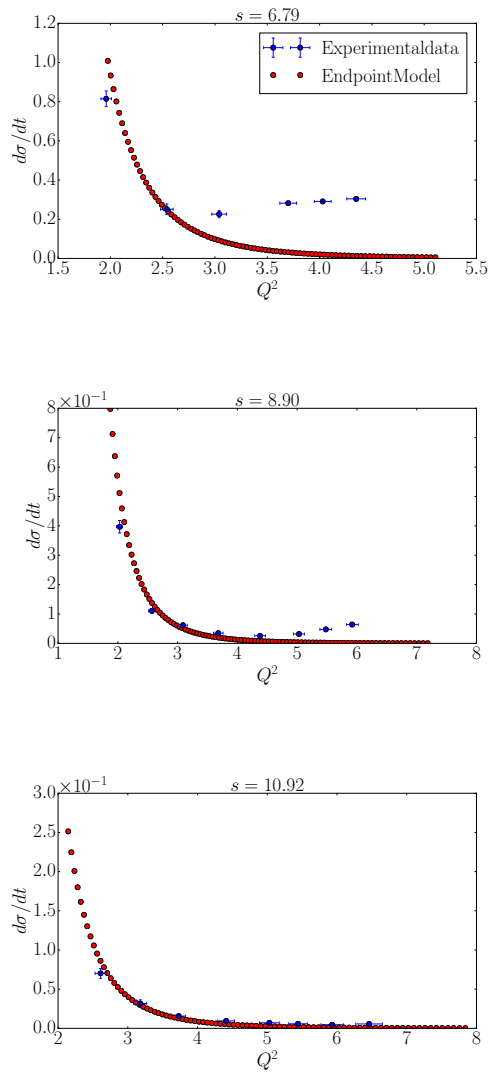


Figure 2: Plot of  $\frac{d\sigma}{dt}$  nbarns/GeV<sup>2</sup> vs  $t$  for  $s = 6.79, 8.90, 10.92$  GeV<sup>2</sup> and  $m = 0.29$  GeV,  $\lambda = 1/2, v = -16, a = 0, t = 45$

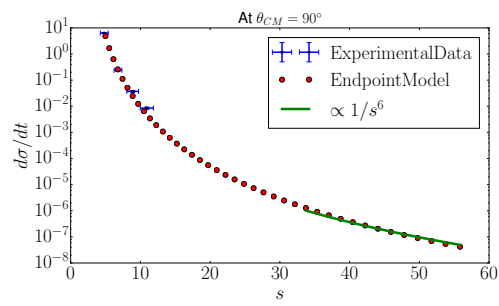


Figure 3: EP evaluation of  $d\sigma/dt \frac{\text{nbarns}}{\text{GeV}^2}$  vs  $s \text{ GeV}^2$  for  $m = 0.29 \text{ GeV}$ ,  $\lambda = 1/2$ ,  $v = -16$ ,  $a = 0$ ,  $t = 45$